

Highly Oriented β -Bi₂O₃-decorated Reduced Graphene Oxide Composites for Supercapacitor Electrodes

Wein-Duo Yang*, Yu-Jiang Lin

Department of Chemical and Materials Engineering, National Kaohsiung University of Science and Technology, Kaohsiung 807, Taiwan, Republic of China.

*E-mail: ywd@nkust.edu.tw

Received: 30 November 2019 / Accepted: 15 January 2020 / Published: 10 February 2020

Highly (201)-oriented β -Bi₂O₃-decorated reduced graphene oxide (rGO) composites were prepared via a novel route using GO and bismuth nitrate as the raw materials in various mass ratios. First, GO solutions were obtained using the improved Hummer's method, and then the highly (201)-oriented β -Bi₂O₃-decorated rGO composites were prepared by novel treatments after a hydrothermal treatment. The galvanostatic charge-discharge measurement results revealed that the composite with a GO: bismuth nitrate mass ratio of 1:1.2 exhibited the maximum specific capacitance of 196 F g⁻¹ at 1 A g⁻¹ in a 1 M KOH electrolyte. The as-obtained electrode maintained a minimum capacitance of 99.6% with excellent reversibility even after 3000 charge-discharge cycles. The electrochemical impedance spectroscopy results revealed that the as-obtained highly (201)-oriented β -Bi₂O₃-decorated rGO composites showed lower impedance and better capacitance performance than rGO. Hence, the findings of this study demonstrated that highly (201)-oriented Bi₂O₃-decorated rGO composites can be used as supercapacitor electrodes.

Keywords: β -bismuth oxide; reduced graphene oxide; improved Hummer's method; capacitance; electrochemical impedance spectroscopy.

1. INTRODUCTION

Owing to their long cycle life, rapid charging, and high-power density, supercapacitors have gained immense attention [1-3]. Various metal oxide semiconductors such as NiO [4], RuO₂ [5], MnO₂ [6], TiO₂ [7], and Bi₂O₃ [8] are used for supercapacitor applications. Among these oxides, nanosized polycrystalline Bi₂O₃ offers large surface area, electrochemical stability, and pseudo-capacitive behavior and might make a significant contribution to the advancement of the supercapacitor technology [9]. Moreover, Bi₂O₃ is an important metal oxide semiconductor. It has been reported that

β - Bi_2O_3 shows better photoactivity than α - Bi_2O_3 owing to its narrower band gap and higher optical absorption in the visible range [10-12].

Gujar et al. [13] synthesized Bi_2O_3 thin films by electrodeposition and achieved a specific capacitance of 98 F g^{-1} in 1 M NaOH at a scan rate of 20 mV s^{-1} . Chitrada et al. developed a facile electrochemical anodization process to deposit nanoporous mixed α/β phase Bi_2O_3 layers on a bismuth metal substrate [14]. The as-obtained Bi_2O_3 layer showed at least two-fold higher specific capacitance than the values reported for electrodeposited α - Bi_2O_3 . Huang et al. [15] synthesized rod-like Bi_2O_3 nanoparticles via a sol-gel method using simple precursor salts. Electrochemical studies showed that rod-like Bi_2O_3 exhibits a specific capacitance of 528 F g^{-1} at a scan rate of 5 mV s^{-1} with a low equivalent series resistance (ESR) value and excellent cyclic stability.

However, a disadvantage of metal oxides is their limited electrical conductivity. The excellent electrical conductivity and high specific area of graphene make it a promising supercapacitor electrode material. Nevertheless, graphene aggregation may occur during the fabrication of electrode materials, leading to the deterioration of its capacitance characteristics. Therefore, transition metal oxides are used as spacers to prevent the aggregation of graphene sheets and improve their capacitance properties [16]. The combination of bismuth oxide and graphene can enhance the electrochemical properties of the overall system.

Activated carbon and Bi_2O_3 composite materials have been used for supercapacitor applications [17-19]. However, the use of graphene/ Bi_2O_3 to improve the capacitance of supercapacitors is very limited. Wang et al. [20] synthesized a graphene nanosheet-bismuth oxide composite in an N, N-dimethyl formamide solution of bismuth cations at $180 \text{ }^\circ\text{C}$. Graphene-bismuth oxide composite electrodes exhibit better capacitive performance than graphene electrodes because of the contribution of bismuth oxide to the total capacitance. Sun et al. [21] reported a novel alkaline rechargeable Ni/Bi battery with high performance. This battery was assembled using $\text{Ni}(\text{OH})_2/\text{graphene}$ and $\text{Bi}_2\text{O}_3/\text{graphene}$ sheets as the positive and negative electrodes, respectively. These sheets were synthesized by chemical deposition methods. The resulting Ni/Bi battery exhibited a high discharge capacity of 102 mAh g^{-1} at a discharge rate of 1 C. Recently, Maruthamani et al. [22] used fine cutting edge-shaped Bi_2O_3 rods/reduced graphene oxide (rGO) nanocomposites for supercapacitor and visible-light photocatalytic applications. The Bi_2O_3 rods/rGO nanocomposites were successfully synthesized using a simple precipitation and calcination method. The Bi_2O_3 rods/rGO composite electrodes exhibited a capacitive performance superior to that of Bi_2O_3 electrodes. Moreover, Deepi et al. [16] prepared pure Bi_2O_3 and graphene/ Bi_2O_3 -based nanocomposite materials via sol-gel methods for supercapacitor applications. They also carried out the physical/electrochemical characterization of the nanocomposites. Because of the presence of carbon and pure Bi_2O_3 , the composites exhibited a high specific capacitance of 136.76 F g^{-1} (at a current density of 0.5 A g^{-1}) and excellent cycling stability ($> 95 \%$ over 1000 cycles).

Composites of rGO/ β - Bi_2O_3 are considered as promising electrode materials for supercapacitor applications. However, since the crystalline temperatures of different bismuth oxide crystal phases are very similar, different polycrystalline phases of Bi_2O_3 or other impurities are often added during the preparation of rGO- β - Bi_2O_3 composite materials. In addition, it is difficult to obtain high-purity rGO-

β -Bi₂O₃ composite materials. To the best of our knowledge, very few reports are available on the preparation of rGO/ β -Bi₂O₃ composite materials for supercapacitor applications.

In this study, we developed a novel route to synthesize highly (201)-oriented β -Bi₂O₃-decorated rGO composites using GO and bismuth nitrate reagents. Furthermore, we characterized the properties of the rGO/ β -Bi₂O₃ composites with different raw material mass ratios.

2. EXPERIMENTAL

2.1. Synthesis of highly (201)-oriented β -Bi₂O₃-decorated rGO composites

GO was prepared using the improved Hummer's method [23]. First, 500 mL of a strongly acidic solution was obtained by mixing sulfuric acid and phosphoric acid in a volume ratio of 9:1. A total of 3 g of natural graphite was added to the above mixture with vigorous agitation. Then, 12 g of potassium permanganate (KMnO₄) was added slowly at 35 °C and the resulting mixture was stirred for 3 h. The reaction temperature was increased to 50 °C with stirring at 600 rpm for 8 h until the mixture turned brownish. Finally, 10 mL of H₂O₂ was poured into the solution to terminate the oxidation of graphite. Finally, brownish-yellow GO was obtained after centrifugation, acid washing, water washing, and vacuum drying.

Various GO:Bi(NO₃)₂·5H₂O mass ratios were used to synthesize the highly (201)-oriented β -Bi₂O₃-decorated rGO composite materials. First, the as-synthesized GO (0.1 g) was mixed with 400 mL of de-ionized water. A certain amount of Bi(NO₃)₂·5H₂O was dissolved in 5 mL of a nitric acid solution. Then, these two solutions were mixed thoroughly. Furthermore, 28 wt.% ammonia water was added to adjust the pH value of the solution at around 8.5. The mixed solution was ultrasonicated and was then autoclaved at 180 °C for 12 h. After the completion of the hydrothermal reaction, the rGO-Bi precursor was removed and washed several times with DI water. Finally, the resulting rGO-Bi precursor was calcined via a two-step reaction as follows.

First, the precursor was dried at a constant temperature of 80 °C for 12 h in a vacuum oven. Subsequently, the dried precursor was placed in a furnace at 450 °C for 2 h and was then naturally cooled under a N₂ atmosphere. When the furnace temperature reached 300 °C, the material was exposed to air. The temperature was then held constant for 30 min and the cooling-down was completed.

2.2. Characterization of the samples

The physical properties of GO and the as-prepared rGO/ β -Bi₂O₃ composites were investigated by X-ray powder diffraction (XRD) (RIGAKU, Rint-2000) with Cu K α radiation ($\lambda = 1.5406 \text{ \AA}$), Raman spectroscopy (HORIBA, HR550) with charge-coupled device (CCD) detection ($-70 \text{ }^\circ\text{C}$), and transmission electron microscopy (TEM) (JEOL, TEM-3010) at an acceleration voltage of 80 kV. Moreover, the surface morphology of the samples was examined by atomic force microscopy (AFM) (BRUKER, Dimension Icon). Thermogravimetric analysis (TGA) was carried out in air (on model TA,

SDT-Q600) using 5–10 mg of the powder samples at a heating rate of 10 °C min⁻¹ up to a maximum temperature of 800 °C.

2.3 Electrochemical measurements

The rGO/ β -Bi₂O₃ mixture with polytetrafluoroethylene as the binder and carbon black as the conductive additive was dispersed in ethanol and was then mixed homogeneously. The resulting slurry was coated onto a current collecting graphite paper. The electrochemical properties of the samples were investigated using a conventional three-electrode cell system in 1 M KOH as the electrolyte by the cyclic voltammetry (CV, CH Instruments, Model 400) method. The galvanostatic charge/discharge (GCD) measurements of the samples were carried out at a constant current density of 1 A g⁻¹ within the same voltage range as that used for the CV measurements. The cycle life of the samples was evaluated using a source meter (Keithley 2400).

3. RESULTS AND DISCUSSION

3.1 Preparation of the rGO/ β -Bi₂O₃ composites

Figure 1 shows the XRD patterns of the rGO/ β -Bi₂O₃ composites with different raw material mass ratios. The broad peak at $2\theta = 22\text{--}26^\circ$ corresponds to rGO. Moreover, the conversion of the sharp and high intensity GO peak at $2\theta = 10^\circ$ (not shown) to a broad, low intensity peak indicates the oxidation of GO through the introduction of oxygen-containing functional groups.

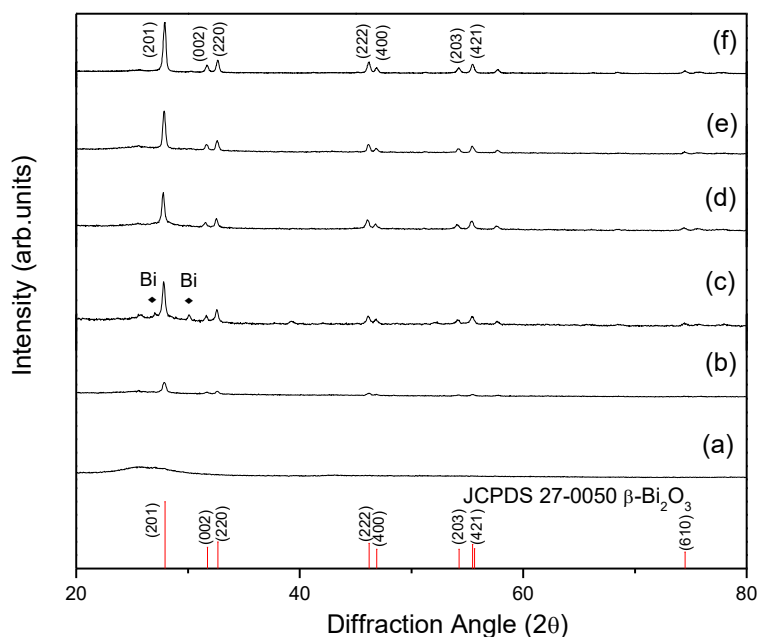


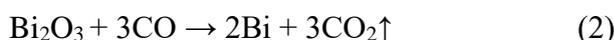
Figure 1. XRD patterns of the rGO/ β -Bi₂O₃ composites with different GO: bismuth nitrate mass ratios. (a) 1:0; (b) 1:0.1; (c) 1:0.3; (d) 1:0.6; (e) 1:0.9; and (f) 1:1.2

This oxidation reaction weakened the van der Waals forces between the graphite layers, resulting in an increase in the interlayer spacing, and hence a shift in the diffraction angle [24]. However, the hydrothermal synthesis involved a high-temperature and high-pressure environment, which eliminated the oxygen-containing functional groups of GO, causing a portion of graphene to wrinkle and stack disorderly. This phenomenon caused a few of the as-produced rGO sheets to regain the (002) crystal plane, resulting in a broad diffraction peak. The diffraction angle shift and the broadening of the peaks confirm the successful preparation of rGO. Figures 1(b)–2(f) show the XRD patterns of the rGO/ β -Bi₂O₃ samples with different raw material mass ratios. The XRD peaks corresponded to the tetragonal phase of β -Bi₂O₃ (JCPDS # 27-0050). With an increase in the amount of Bi (by adding the Bi-precursor), the β -Bi₂O₃ content of the rGO/ β -Bi₂O₃ samples also increased. In the rGO/ β -Bi₂O₃ samples, the broad peak at $2\theta = 23\text{--}26^\circ$ characteristic of rGO could not be observed clearly because it was obscured by the stronger diffraction peak of β -Bi₂O₃.

Furthermore, the relative intensity of the diffraction peak corresponding to the (201) plane ($2\theta =$ approximately 27.8°) was much stronger than that of the peaks corresponding to the other planes, indicating that β -Bi₂O₃ was oriented along the (201) plane (compare to JCPDS # 27-0050). The sharp and well-defined peaks of the as-prepared powders indicate that they consisted of highly (201)-oriented β -Bi₂O₃ particles. This observation is consistent with that reported by Huang et al. [15].

It can be observed from Figure 1(c) that the rGO/ β -Bi₂O₃ samples consisted of a small amount of Bi. The rGO/ β -Bi₂O₃ preparation mechanism can be elucidated as follows.

Carbon in the form of graphene was used to reduce amorphous Bi₂O₃ to Bi during the first step of the heat treatment, as shown in reactions (1) and (2). The bismuth metal was then oxidized during the cooling process at a certain temperature to produce β -Bi₂O₃ with fewer impurities (second step of the heat treatment process), as shown in reaction (3). The formation of β -Bi₂O₃ occurred as shown in reactions (1), (2), and (3).



Finally, rGO/ β -Bi₂O₃ composites with different GO: bismuth nitrate mass ratios (1:0, 1:0.1, 1:0.3, 1:0.6, 1:0.9, and 1:1.2) were obtained.

In this study, the high temperature and pressure of the aqueous solution in the closed system facilitated the dissociation or dissolution of the oxygen-containing functional groups to achieve the reduction effect. Furthermore, because the reaction proceeded without the addition of a reducing agent, the production of rGO/ β -Bi₂O₃ was relatively simple and required no further treatment.

Figure 2 shows the Raman shift of the rGO/ β -Bi₂O₃ composites with different raw material mass ratios. According to Andrea et al. [25], the characteristic peak of the G band of graphene represents the vibrational mode of sp²-hybridized carbon atoms. Therefore, the G band position of graphene is very sensitive to the change in its number of layers. With a decrease in the number of graphene layers, the G band shifts toward higher wavenumbers and vice versa.

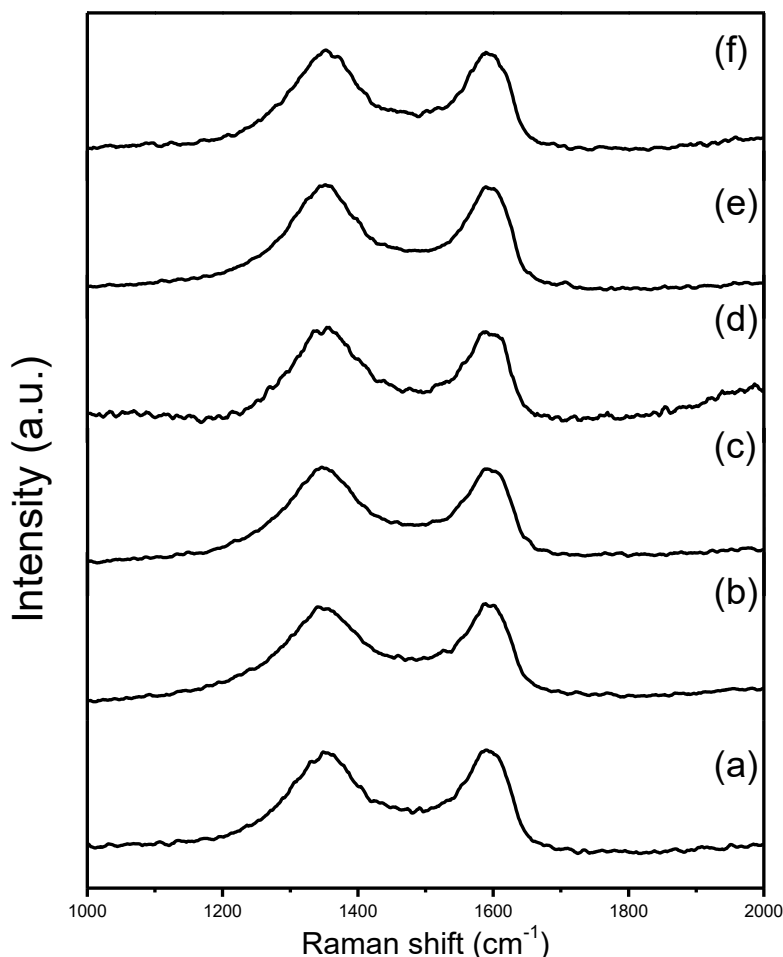


Figure 2. Raman shifts of the rGO/ β -Bi₂O₃ composites with different GO: bismuth nitrate mass ratios. (a) 1:0; (b) 1:0.1; (c) 1:0.3; (d) 1:0.6; (e) 1:0.9; and (f) 1:1.2

The R value of GO was found to be 0.87. This indicates that the GO prepared in this study showed higher regularity and lower randomness than that prepared under other conditions. The G band at 1597.9 cm⁻¹ confirms the introduction of oxygen-containing functional groups on GO. These groups increased the distance between the graphite sheet layers and undermined the interlayer structure. However, it is worth mentioning that the large number of oxygen-containing functional groups in the interlayer structure decreased the conductive performance of GO [26]. The rGO prepared by the hydrothermal synthesis method showed a highly stacked sp² structure because of the elimination of the oxygen-containing functional groups, causing an increase in the reduction of graphite and a shift in the G band to 1585.5 cm⁻¹.

The properties and quality of graphene can be evaluated by monitoring the shifts in its D and G bands. The electrical conductivity and charge storage capacity of graphene can also be characterized using its Raman spectrum. The GO prepared in this study exhibited a G band Raman shift to a higher wavenumber offset, demonstrating a thin-layer (fewer layers) graphene structure. The lowest R value indicates the ordered arrangement of the graphene structure.

With an increase in the $\beta\text{-Bi}_2\text{O}_3$ content of the rGO/ $\beta\text{-Bi}_2\text{O}_3$ samples, their R value increased, presumably because some impurities and defects were introduced during the preparation of the samples. Moreover, the loaded $\beta\text{-Bi}_2\text{O}_3$ particles damaged the graphene order. However, as the G band shift of graphene is highly sensitive to its thickness, the relative thickness of the graphene sheets could be measured from the displacement of their G band position. The rGO/ $\beta\text{-Bi}_2\text{O}_3$ sample with the GO: bismuth nitrate mass ratio of 1:0.6 exhibited the highest G band wavenumber of 1590.8 cm^{-1} , indicating that the graphene produced in this study showed the highest degree of exfoliation and conductivity at this Bi content.

3.2 Morphologies of the as-prepared rGO/ $\beta\text{-Bi}_2\text{O}_3$ composites

Figure 3 shows the TEM image of the rGO/ $\beta\text{-Bi}_2\text{O}_3$ composite with the GO: bismuth nitrate mass ratio of 1:1.2. The black particles in Figure 3(a) correspond to $\beta\text{-Bi}_2\text{O}_3$ nanoparticles, while the transparent wrinkles correspond to rGO. As can be observed from the figure, the $\beta\text{-Bi}_2\text{O}_3$ nanoparticles were distributed on the graphene sheet surfaces, while rGO exhibited significant bulging and wrinkling at the $\beta\text{-Bi}_2\text{O}_3$ -containing sites. Hence, the $\beta\text{-Bi}_2\text{O}_3$ nanoparticles replaced the oxygen-containing functional groups and induced the rGO layer exfoliation effect. Figure 3(b) shows the electron diffraction pattern of graphene, exhibiting a light graphene ring with insufficient intensity, which is attributed to the scattering effect of electron diffraction for the different layers of graphene. Figure 3(c) shows the electron diffraction pattern of the $\beta\text{-Bi}_2\text{O}_3$ particles.

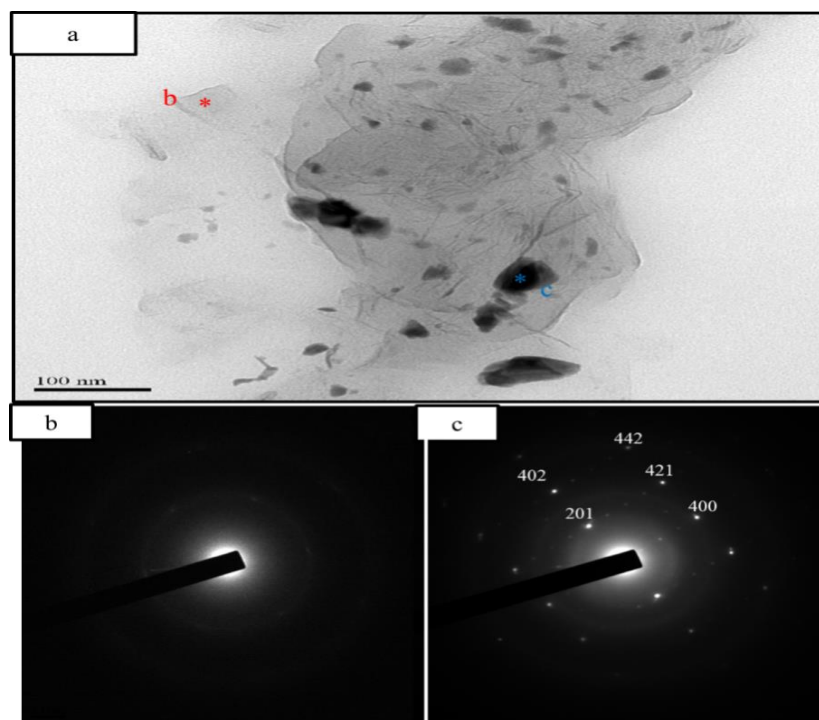


Figure 3. TEM image of the rGO/ $\beta\text{-Bi}_2\text{O}_3$ composite with the GO: bismuth nitrate mass ratio of 1:1.2. (a) TEM image of rGO/ $\beta\text{-Bi}_2\text{O}_3$; (b) electron diffraction pattern of rGO; and (c) electron diffraction pattern of $\beta\text{-Bi}_2\text{O}_3$

The electron diffraction pattern exhibited clear spots highly oriented along the (201) plane. This indicates that the β - Bi_2O_3 particles corresponded to the crystal plane of the β - Bi_2O_3 phase [27]. The XRD results and electron diffraction patterns confirm the successful synthesis of highly (201)-oriented β - Bi_2O_3 -decorated rGO composites.

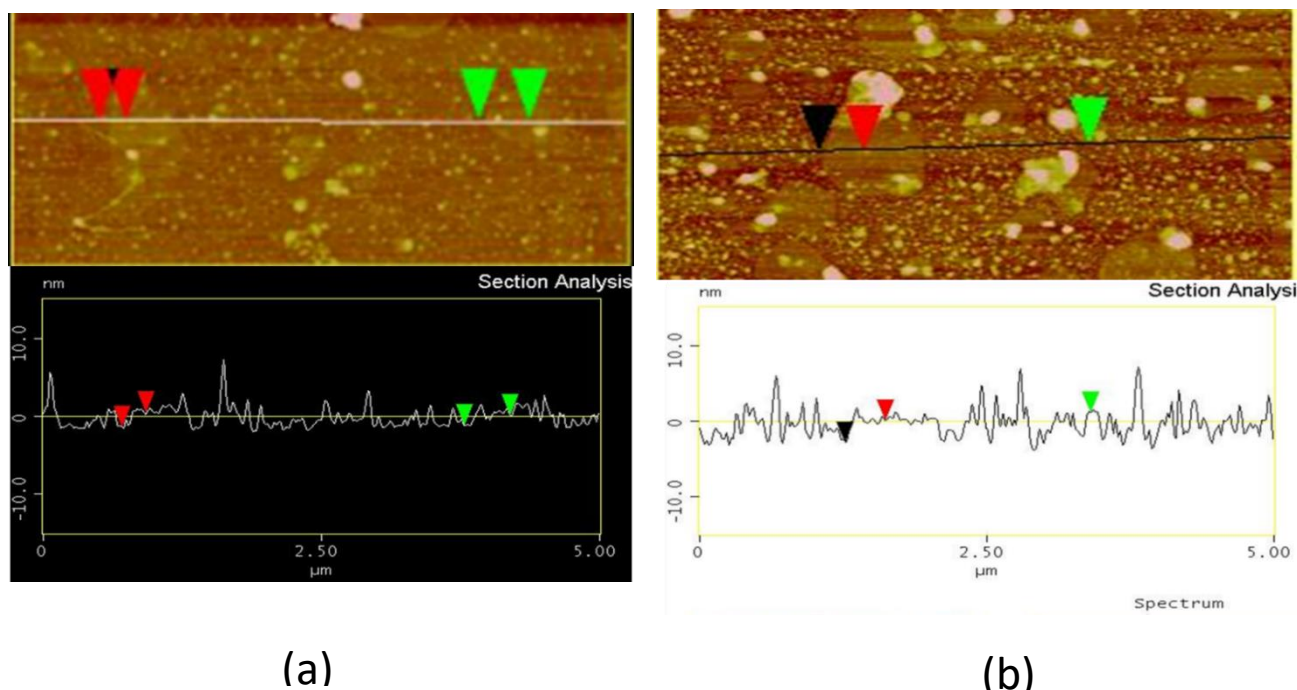


Figure 4. AFM images of rGO and rGO/ β - Bi_2O_3 . (a) rGO; (b) rGO/ β - Bi_2O_3 composite with the GO: bismuth nitrate mass ratio of 1:1.2

The graphene materials were dispersed in absolute alcohol and were deposited on a glass substrate for surface morphology analysis. Figure 4 shows the AFM images of rGO and the rGO/ β - Bi_2O_3 samples. It was found that rGO exhibited a fragmented distribution. The hydrothermal method resulted in the exfoliation of graphene on the graphite sheet during the reaction. The disordered stacking of rGO occurred during the reduction process. The thickness of rGO was approximately 1.1–2.2 nm and the number of layers was 2–6 (Figure 4(a)). Figure 4(b) shows the AFM image of the as-prepared rGO/ β - Bi_2O_3 composite with the GO: bismuth nitrate mass ratio of 1:0.6. Some particles were observed on the surface of the graphene sheets, indicating that β - Bi_2O_3 was successfully synthesized. The thickness of rGO/ β - Bi_2O_3 was higher than that of rGO, indicating that β - Bi_2O_3 facilitated the interlayer exfoliation while avoiding the agglomeration of graphene. However, because of the loading of β - Bi_2O_3 particles, the thickness of graphene was more than that of rGO, which showed a thickness of 2.2–4.2 nm and approximately 4–8 layers.

3.3 Electrochemical properties

Figure 5 shows the CV curves of the GO, rGO, and rGO/ Bi_2O_3 samples at the scanning rate of 50 mV s^{-1} . It can be observed from the figure that the main charge storage mechanism of GO was the

formation of an electric double layer, and its C-V curve was rectangular. However, the interlayer and surface of GO consisted of a large amount of oxygen-containing functional groups, which significantly decreased its electrical conductivity. Moreover, the hydrophilic character of GO gradually deteriorated in the aqueous electrolyte. The CV curve of rGO showed a significant decrease in its oxygen-containing functional groups because of the reduction reaction under the high-temperature and high-pressure environment of the hydrothermal system. This decrease in the number of oxygen-containing functional groups of rGO increased the degree of wetting between the electrode and the electrolyte, thereby improving its conductivity. Energy storage in rGO also occurred via an electric double layer. In the case of the rGO/ β -Bi₂O₃ composites, the composited Bi₂O₃ not only contributed to the conductivity of graphene, but also enhanced the charge storage effect of the electrode material.

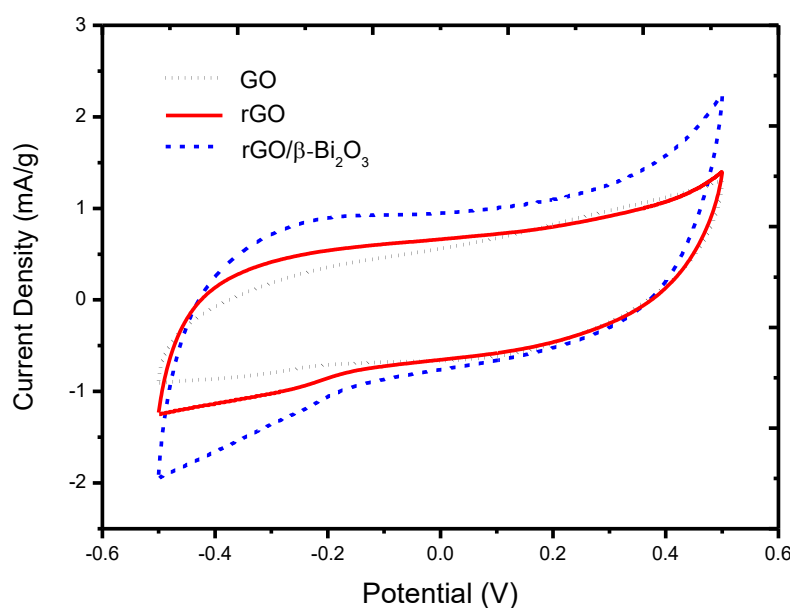


Figure 5. CV curves of the GO, rGO, and rGO/Bi₂O₃ samples at the scanning rate of 50 mV s⁻¹

Figure 6 shows the CV curves of the as-prepared rGO/ β -Bi₂O₃ composites with different GO:bismuth nitrate mass ratios at the scanning rate of 75 mV s⁻¹. The CV area of the electrodes increased with an increase in their bismuth content. This indicates that the capacitive ability of the rGO/ β -Bi₂O₃ electrodes increased with an increase in their bismuth content. With an increase in the bismuth content, the contribution of the pseudo-capacitance of Bi₂O₃ to the total capacitance of the rGO/Bi₂O₃ composites increased gradually. Nevertheless, the rGO/ β -Bi₂O₃ composites prepared in this study were mainly electric double layers capacitive (EDLC) and slightly pseudo-capacitive [28, 29].

Figure 7 shows the GCD characteristic curves of the GO, rGO, and rGO/ β -Bi₂O₃ samples. The specific capacitance of the samples was calculated from their discharge curves using equation (4):

$$C_m = \frac{i \times \Delta t}{\Delta V \times m} \quad (4)$$

where i (A) is the discharge current, Δt (s) is the discharge time, ΔV (V) is the voltage potential, and m (g) is the mass of the active materials.

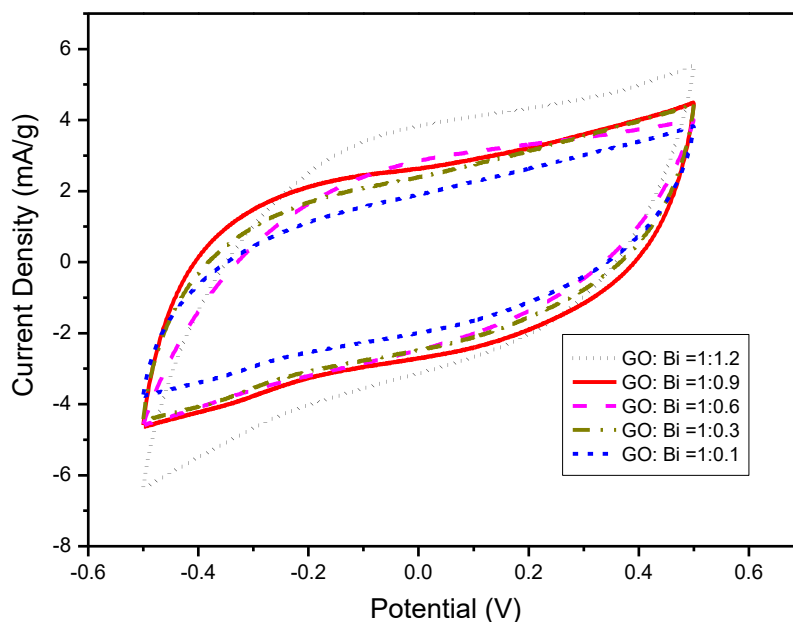


Figure 6. CV curves of the rGO/ β -Bi₂O₃ electrodes with different GO: bismuth nitrate mass ratios at the scanning rate of 75 mV s⁻¹. (a) GO: bismuth nitrate = 1:0.1; (b) GO: bismuth nitrate = 1:0.3; (c) GO: bismuth nitrate = 1:0.6; (d) GO: bismuth nitrate = 1:0.9, and (d) GO: bismuth nitrate = 1:0.6; (d) GO: bismuth nitrate = 1:1.2

GO showed a low capacitance at 50 F g⁻¹, as shown in Figure 7(a). This can be attributed to the presence of a large number of oxygen-containing functional groups in it, which affected the electrical conductivity of graphene. In contrast, the G band of rGO appeared at 1585.5 cm⁻¹, indicating the absence of the GO stabilizing factor, resulting in the agglomeration of the graphene layers after the hydrothermal synthesis [30]. This indicates that in rGO, repeated decomposition and reconstruction of the atomic-scale structures occurred during the reduction process, leading to an increase in the number of defects and a decrease in the graphene order, which increased its R value. The capacitance of rGO was 84.6 F g⁻¹, as shown in Figure 7(b). Furthermore, the capacitance of the rGO/ β -Bi₂O₃ sample with the GO: bismuth nitrate mass ratio of 1:1.2 increased to 196 F g⁻¹, as shown in Figure 7 (c). This indicates that in the rGO/ β -Bi₂O₃ samples, graphene showed charge storage capacity by forming a composite with β -Bi₂O₃. With the addition of the metal oxide, the contribution of the pseudo-capacitance of β -Bi₂O₃ to the capacitance of the rGO/ β -Bi₂O₃ composites increased [16].

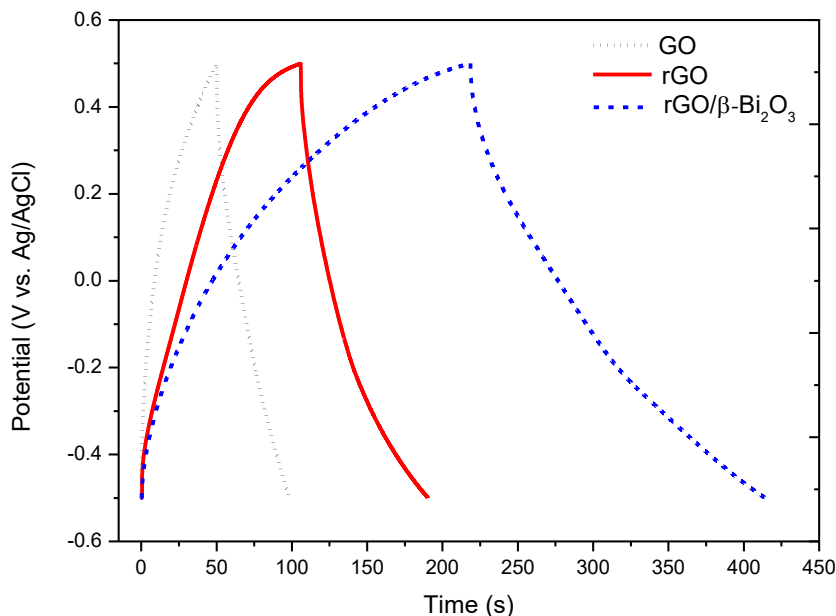


Figure 7. GCD curves of the GO, rGO, and rGO/ β -Bi₂O₃ samples at 1 A g⁻¹. (a) GO, (b) rGO, and (c) rGO/ β -Bi₂O₃

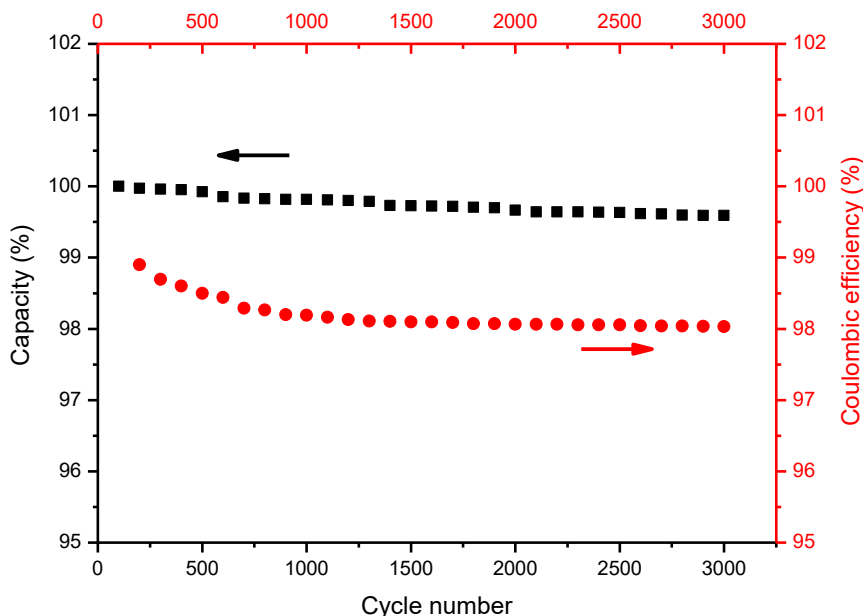


Figure 8. The cycle life of the rGO/ β -Bi₂O₃ composite with the GO: bismuth nitrate mass ratio of 1:1.2 at 1 A g⁻¹. (a) capacitance retention; (b) Coulombic efficiency

Figure 8 shows the cycle life of the rGO/ β -Bi₂O₃ composite with the GO: bismuth nitrate mass ratio of 1:1.2 at 1 A g⁻¹. The composite showed a capacitance retention of 99.6% or more after 3000 charge-discharge cycles, as shown in Figure 8 (a). This indicates that this composite showed excellent reversibility. The Coulombic efficiency of a material, which is mainly used to evaluate the reversibility of the adsorbed and desorbed electrons on it, can be used to evaluate its electron transfer and

capacitance stability [31]. Figure 8(b) shows that the rGO/ β -Bi₂O₃ composite with the GO: bismuth nitrate mass ratio of 1:1.2 maintained a Coulombic efficiency of 98% after 3000 charge-discharge cycles.

Table 1 shows a comparison of electrochemical performance of bismuth oxide-based electrode in the literature. Galvanostatic charge-discharge measurement results revealed that the composite with a GO: bismuth nitrate mass ratio of 1:1.2 exhibited the specific capacitance of 196 F g⁻¹ at 1 A g⁻¹ in a 1 M KOH electrolyte and an excellent capacitance retention of 99.6% after 3000 charge-discharge cycles. The capacitance retention is quite higher than that of the previously studied electrode material.

Table 1. A comparison of electrochemical performance of bismuth oxide-based electrode in the literature

Material	Electrolyte	Current density (A g ⁻¹)	Capacitance retention (%)	Specific capacitance (F g ⁻¹)	Ref
rGO/ α -Bi ₂ O ₃	6 M KOH	0.5	95 (1000 cycles)	136.76	[16]
β -Bi ₂ O ₃ /AC	6 M KOH	1	59 (1000 cycles)	332.6	[17]
α -Bi ₂ O ₃ /AC	1 M Li ₂ SO ₄			99.5	[18]
β -Bi ₂ O ₃ /graphene	6 M KOH	1	65 (1000 cycles)	255	[20]
rGO/ α -Bi ₂ O ₃	6 M KOH	2	94 (1000 cycles)	1041	[22]
rGO/ β -Bi ₂ O ₃	6 M KOH	1		617.1	[33]
rGO/ β -Bi ₂ O ₃	1 M KOH	1	99.6 (3000 cycles)	196	This work

AC: activated carbon

Electrochemical impedance spectroscopy (EIS) utilizes a small AC voltage or current disturbance to investigate the electrochemical properties of a material. From the AC impedance data of an electrode, its equivalent circuit diagram can be simulated to calculate the corresponding electrode reaction parameters. In general, Nyquist plots extend from the divergent section of the low frequency section to the intercept of the X axis ($Z'(\Omega)$).

The enclosed high-frequency section can be considered as the total impedance (R_t) of the tested component and the total component Impedance (R_t) is the sum of the three impedances, as follows [32]:

$$R_t = R_s + R_c + R_p \quad (5)$$

where R_s represents the ion mobility of the electrolyte and R_c and R_p represent the charge transfer resistance and ion mass transfer impedance of the electrode, respectively.

Figure 9 shows the impedance analysis of the rGO and rGO/ β -Bi₂O₃ (GO: bismuth nitrate mass ratio = 1:1.2) electrodes. The rGO/ β -Bi₂O₃ electrode exhibited a smaller semicircular diameter at high frequencies, indicating that it exhibited low R_c impedance and excellent charge transfer ability. The rGO/ β -Bi₂O₃ electrode exhibited lower R_s impedance than the rGO electrode because of the presence of β -Bi₂O₃ particles in it, which effectively exfoliated graphene and enhanced the infiltration of the electrolyte into the voids of the rGO layers [33]. In addition, the low frequency part represents the

diffusion resistance of the electrolyte ions in the pores of the electrodes. The rGO/ β -Bi₂O₃ composite showed an approximately straight line with slope more than 45°, indicating its excellent capacitive properties.

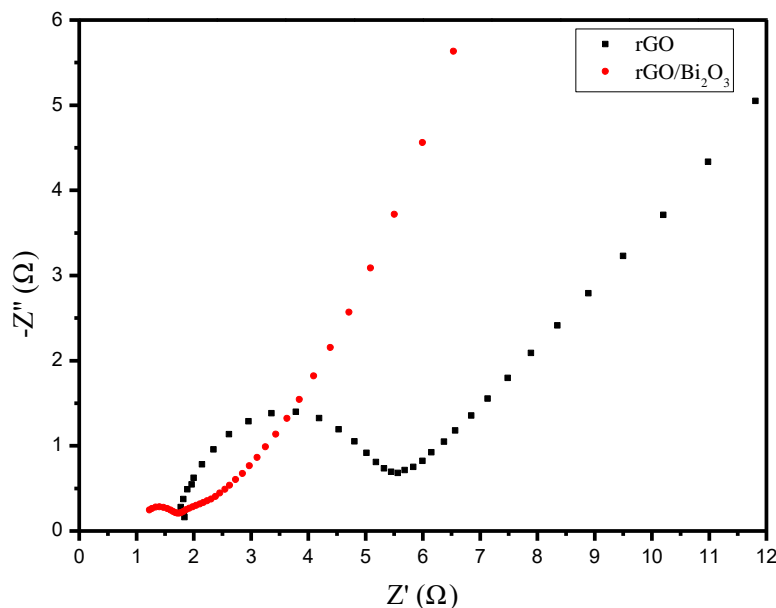


Figure 9. Impedance analysis of rGO and the rGO/ β -Bi₂O₃ electrode with the GO: bismuth nitrate mass ratio of 1:1.2

4. CONCLUSIONS

Highly (201)-oriented β -Bi₂O₃-decorated rGO composites with various GO: bismuth nitrate mass ratios were prepared via a hydrothermal route. First, GO solutions were obtained using the improved Hummer's method, and then the rGO/ β -Bi₂O₃ composites were prepared by a novel two-step reaction after the hydrothermal treatment. The physicochemical and electrochemical properties of the rGO/ β -Bi₂O₃ composites were investigated.

During the preparation, the oxygen-containing functional groups of the as-prepared rGO/ β -Bi₂O₃ composites were largely eliminated, indicating the successful reduction of GO to rGO. Moreover, with an increase in the β -Bi₂O₃ content, the surface morphology of graphene changed from coil-shaped to lamellar. The thickness of the rGO/ β -Bi₂O₃ composites was affected by the β -Bi₂O₃ particles. The rGO/ β -Bi₂O₃ composites showed a thickness of 2.2–4.2 nm and consisted of approximately 4–8 layers. Moreover, the GCD measurements revealed that the rGO/ β -Bi₂O₃ composite with the GO: bismuth nitrate mass ratio of 1:1.2 exhibited a maximum capacitance of 196 F g⁻¹ at 1 A g⁻¹ in a 1 M KOH electrolyte. This composite showed a retention ratio and charge-discharge efficiency of 99.6% after 3000 charge-discharge cycles. The rGO/ β -Bi₂O₃ composites exhibited lower total resistance and better mass transfer performance than rGO. Hence, the rGO/ β -Bi₂O₃ composites prepared by the novel two-step heat treatment in this study are suitable for supercapacitor applications.

ACKNOWLEDGEMENTS

The authors thank the Ministry of Science and Technology of Taiwan for the financial support (No. 107-2221-E-992-030).

CONFLICT OF INTEREST

The authors declare that they have no conflict of interest.

References

1. C. Peng, S. Zhang, D. Jewell, and G. Z. Chen, *Progress in Natural Science*, 18 (2008) 777.
2. V. Augustyn, P. Simon, and B. Dunn, *Energy & Environmental Science*, 7 (2014) 1597.
3. J. Xia, F. Chen, J. Li, and N. Tao, *Nat. Nanotechnol.*, 4 (2009) 505.
4. S.-I. Kim, J.-S. Lee, H.-J. Ahn, H.-K. Song, and J.-H. Jang, *ACS Appl. Mater. Interfaces*, 5 (2013) 1596.
5. T. Liu, W.G. Pell, and B.E. Conway, *Electrochimica Acta*, 42 (1997) 3541.
6. M. Kundu, L. Liu, *Journal of Power Sources*, 243 (2013) 676.
7. X. Lu, G. Wang, T. Zhai, M. Yu, J. Gan, Y. Tong, and Y. Li, *Nano Lett.*, 12 (2012) 1690.
8. F.-L. Zheng, G.-R. Li, Y.-N. Ou, Z.-L. Wang, C.-Y. Su, and Y.-X. Tong, *Chem. Commun.*, 46 (2010) 5021.
9. R. Liu, L. Ma, G. Niu, X. Li, E. Li, Y. Bai, and G. Yuan, *Advanced Functional Materials*, 2017; <https://doi.org/10.1002/adfm.201701635>.
10. J. Yang, T. Xie, C. Liu, L. Xu, *Materials*, 11 (2018) 1359.
11. M. Suresh, A. Sivasamy, *Journal of Environmental Chemical Engineering*, 6 (2018) 3745.
12. K. C. Chitrada, K. S. Raja, R. Gakhar, and D. Chidambaram, *Journal of the Electrochemical Society*, 162 (2015) H380.
13. T.P. Gujar, V.R. Shinde, C.D. Lokhande, and S.-H. Han, *Journal of Power Sources*, 161 (2006) 1479.
14. K. C Chitrada, S R. Krishnan, *ECS Transactions*, 61 (2014) 55.
15. X. Huang, W. Zhang, Y. Tan, J. Wu, Y. Gao, and B. Tang, *Ceramics International*, 42 (2016) 2099.
16. S. Nagarani, G. Sasikala, K. Satheesh, M. Yuvaraj, and R. Jayavel, *Journal of Materials Science*, 29 (2018) 11738.
17. S.X. Wang, C.C. Jin, and W.J. Qian, *Journal of Alloys and Compounds*, 615 (2014) 12.
18. S.T. Senthilkumar, R. Kalai Selvan, M. Ulaganathan, and J.S. Melo, *Electrochimica Acta*, 115 (2014) 518.
19. N.N. Xia, D.S. Yuan, T.X. Zhou, J. Chen, S. Mo, and Y. Liu, *Mater. Res. Bull.*, 46 (2011) 687.
20. H.-W. Wang, Z.-A. Hu, Y.-Q. Chang, Y.-L. Chen, Z.-Q. Lei, Z.-Y. Zhang, and Y.-Y. Yang, *Electrochimica Acta*, 55 (2010) 8974.
21. J. Sun, Z. Li, J. Wang, W. Hong, P. Gong, P. Wen, Z. Wang, and S. Yang, *Journal of Alloys and Compounds*, 643 (2015) 231.
22. D. Maruthamani, S. Vadivel, M. Kumaravel, B. Saravanakumar, B. Paul, S. S. Dhar, A. Habibi-Yangjeh, A. Manikandan, and G. Ramadoss, *Journal of Colloid and Interface Science*, 498 (2017) 449.
23. J. Chen, B. Yao, C. Li, and G. Shi, *Carbon*, 64 (2013) 225.
24. H. Hu, X. Wang, J. Wang, L. Wan, F. Liu, H. Zheng, R. Chen, and C. Xu, *Chemical Physics Letters*, 484 (2010) 247.
25. S. Sekhar, M. J. Kim, K. S Yeom, S. S. A. An, H. Ju, and D. K. Yi, *Trends Anal. Chem.*, 80 (2016) 125.
26. W.-D. Yang, Y.-R. Li, and Y.-C. Lee, *Applied Surface Science*, 380 (2016) 249.

27. H. W. Kim, *Thin Solid Films*, 516 (2008) 3665.
28. H. Shen, Y. Zhang, X. Song, Y. Liu, H. Wang, H. Duan, and X. Kong, *Journal of Alloys and Compounds*, 770 (2019) 926.
29. S. Shahrokhian, R. Mohammadi, and E. Asadian, *International Journal of Hydrogen Energy*, 41 (2016) 17496.
30. J. Shen, Y. Hu, C. Li, C. Qin, and M. Ye, *Smal.*, 5 (2009) 82.
31. M. Y. Han, J. C. Brant, and P. Kim, *Phys. Rev. Lett.*, 104 (2010) 056801.
32. Z. Lei, J. Zhang, and X. S. Zhao, *J. Mater. Chem.*, 22 (2012) 153.
33. S. Liu, Y. Wang, Z. Ma, *Int. J. Electrochem. Sci.*, 13 (2018) 12256.

© 2020 The Authors. Published by ESG (www.electrochemsci.org). This article is an open access article distributed under the terms and conditions of the Creative Commons Attribution license (<http://creativecommons.org/licenses/by/4.0/>).